ANTIOXIDANTS & REDOX SIGNALING
Volume 19, Number 8, 2013

DOI: 10.1089/ars.2012.4831

Therapeutics

ORIGINAL RESEARCH COMMUNICATION

# Downregulation of Tumor Growth and Invasion by Redox-Active Nanoparticles

Lirija Alili,[1,*] Maren Sack,[1,*] Claudia von Montfort,[1,2] Shailendra Giri,[3] Soumen Das,[4] Kate S. Carroll,[5] Klaus Zanger,[6] Sudipta Seal,[4] and Peter Brenneisen[1]

## Abstract

***Aims:*** Melanoma is the most aggressive type of malignant skin cancer derived from uncontrolled proliferation of melanocytes. Melanoma cells possess a high potential to metastasize, and the prognosis for advanced melanoma is rather poor due to its strong resistance to conventional chemotherapeutics. Nanomaterials are at the cutting edge of the rapidly developing area of nanomedicine. The potential of nanoparticles for use as carrier in cancer drug delivery is infinite with novel applications constantly being tested. The noncarrier use of cerium oxide nanoparticles (CNPs) is a novel and promising approach, as those particles *per se* show an anticancer activity *via* their oxygen vacancy-mediated chemical reactivity. ***Results:*** In this study, the question was addressed of whether the use of CNPs might be a valuable tool to counteract the invasive capacity and metastasis of melanoma cells in the future. Therefore, the effect of those nanoparticles on human melanoma cells was investigated *in vitro* and *in vivo*. Concentrations of polymer-coated CNPs being nontoxic for stromal cells showed a cytotoxic, proapoptotic, and anti-invasive capacity on melanoma cells. *In vivo* xenograft studies with immunodeficient nude mice showed a decrease of tumor weight and volume after treatment with CNPs. ***Innovation:*** In summary, the redox-active CNPs have selective pro-oxidative and antioxidative properties, and this study is the first to show that CNPs prevent tumor growth *in vivo*. ***Conclusion:*** The application of redox-active CNPs may form the basis of new paradigms in the treatment and prevention of cancers. *Antioxid. Redox Signal*. 19, 765–778.

## Introduction

Reactive oxygen species (ROS) are byproducts of cellular metabolism, generated primarily by mitochondrial activity, other endogenous (52, 53) or exogenous sources such as xenobiotics (25), cytostatics (49, 65), as well as UV radiation (9). A variety of soluble factors stimulate the generation of ROS, which *via* alterations of the intracellular redox state and/or oxidative modification of proteins exert their action on signaling components (59, 60). If not regulated properly by, for example, antioxidants, excess ROS result in oxidative stress, thus damaging cellular macromolecules and inhibiting cellular functions that may result in some pathologies, including cancer (47, 63).

The number of malignant melanoma being the most aggressive type of skin cancer is rapidly increasing, suggesting a doubling of the incidence every 10–20 years (18, 24). Although surgical treatment of early melanoma leads to high cure rates, the prognosis of 5-year survival for advanced melanoma is rather poor (4), as a chronic increased level of ROS favors survival and proliferation (16, 64). Those melanomas tend to metastasize and show some resistance to classical treatments (7). This reflects the current lack of therapeutic approaches for treating advanced melanoma (19). In addition,

[1]Medical Faculty, Institute of Biochemistry & Molecular Biology I, Heinrich-Heine-University, Duesseldorf, Germany.
[2]Department of Cell Death and Proliferation, IIBB-CSIC, Barcelona, Spain.
[3]Department of Experimental Pathology, Mayo Clinic College of Medicine, Rochester, Minnesota.
[4]Advanced Materials Processing and Analysis Center, Nanoscience and Technology Center (NSTC), Mechanical, Materials Aerospace Engineering (MMAE), University of Central Florida, Orlando, Florida.
[5]TSRI, Department of Chemistry, Jupiter, Florida.
[6]Medical Faculty, Institute of Anatomy II, Heinrich-Heine-University, Duesseldorf, Germany.
*These two authors contributed equally to this work.

### Innovation

As both the incidence of melanoma is increasing faster than that of other cancers, and the chemotherapeutical treatment of a majority of patients with metastatic melanoma often results in adverse reactions and response rates that are not high enough to significantly affect median survival, novel therapeutical approaches must be the objective for the near future. In this study, we have shown for the first time *in vitro* and *in vivo* that concentrations of polymer-coated cerium oxide nanoparticles (CNPs) being nontoxic for stromal cells exhibit a direct reactive oxygen species-dependent cytotoxic (proapoptotic) and anti-invasive effect on melanoma cells. Our study highlights a prospective clinical significance of CNPs.

epidemiological studies showed an increased risk of secondary cancers in individuals having a history of cutaneous melanoma (35). These facts pose a great challenge for finding new approaches for the chemoprevention of the progression of that type of cancer. Breaking ROS tolerance of melanoma cells by either impairing their antioxidant system or further elevating their intracellular ROS level by new therapeutics might hold a future promise as an alternative therapeutical approach.

Nanomedicine, the medical application of nanotechnology, deals with the application of structures < 100 nm as a valuable set of research tools in anticancer therapy (15) in the near future. A nanoparticle-based therapy may have the potential as supplemental therapy supporting the classical anticancer strategies. If future studies show that a nanoparticle-based anticancer therapy is as effective as established therapies and has less side effects, the application of nanoparticles as a major anticancer approach is conceivable. In earlier studies, vacancy engineered cerium oxide ($CeO_2$)-based nanoparticles exhibited superoxide dismutase (SOD)- and catalase-mimetic activity in a cell-free system (27, 44).

In this study, it was addressed whether polymer-coated cerium oxide nanoparticles (CNPs) might be a valuable therapeutical tool to combat invasive capacity and metastasis of melanoma cells. For that, *in vitro* and *in vivo* studies were performed, resulting in promising data.

## Results

To decide on the use of uncoated or dextran-coated CNP as a potential therapeutical tool to lower tumor invasion and metastasis *in vitro* and *in vivo*, the effect of both types of these nanoparticles on the expression of α-smooth muscle actin (αSMA), a biomarker of myofibroblastic cells promoting tumor invasion (13), and on the viability of tumor cells was tested. Transforming growth factor (TGFβ1) significantly increased the amount of the αSMA protein compared to the untreated controls. That TGFβ1-mediated αSMA expression could completely be abrogated by dextran-coated CNP, but not uncoated CNP. The polymer dextran had no effect on αSMA expression (Fig. 1A). These data indicate the use of coated CNP to prevent a myofibroblast-dependent increase in tumor invasion. Furthermore, the treatment of melanoma cells with coated or uncoated CNPs increased cell death of the tumor cells. However, it is interesting that the coated CNPs showed a slightly stronger effect in context of cell toxicity (Fig. 1B). In conclusion, the dextran-coated nanoparticles showed a more promising effect regarding the tested parameters.

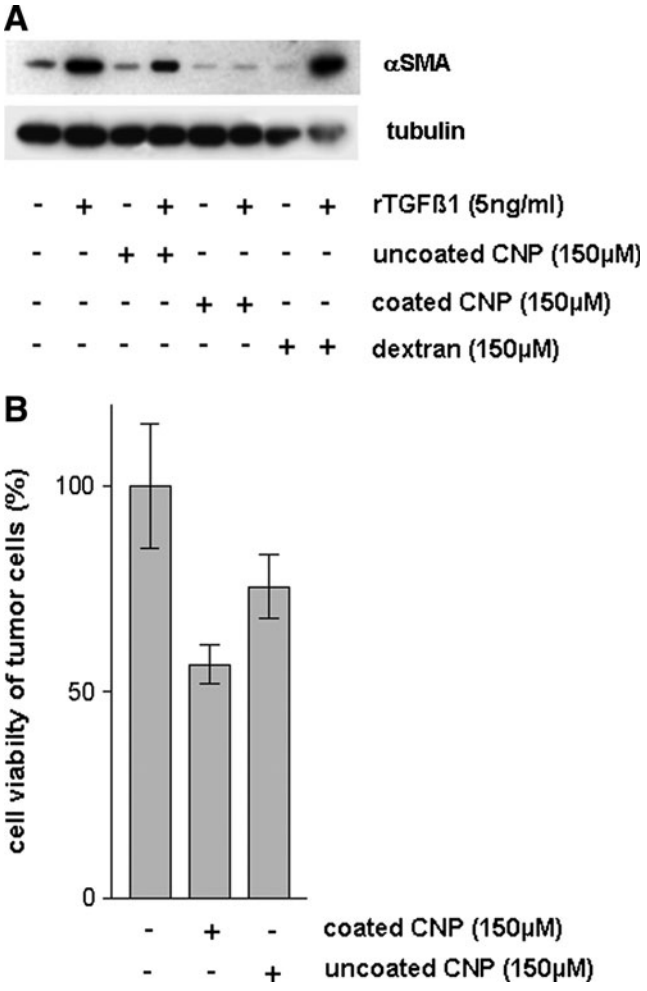


**FIG. 1. Effect of coated *versus* uncoated cerium oxide nanoparticles (CNP) *in vitro*. (A)** Dextran-coated nanoparticles lower α-smooth muscle actin (αSMA) expression. Subconfluent human dermal fibroblasts (HDFs) were either mock-treated or pretreated for 48 h with 150 μm coated or uncoated CNPs before addition of recombinant transforming growth factor β1 (rTGFβ1). TGFβ1 and the cerium oxide particles were present for an additional 48 h; α-tubulin was used as a loading control. Three independent experiments were performed. **(B)** Coated and uncoated nanoparticles lower cell viability of melanoma cells. Subconfluent melanoma cells (A375) were treated with coated or with uncoated CNPs or untreated (ct). The percentage of living cells after 96 h was measured by MTT assay. The experiments were performed in two independent experiments with triplicates in each group.

Therefore, for further experiments, this study focused on the importance of polymer-coated CNPs as a potential anticancer agent for prevention of invasion of tumor cells *in vivo* and *in vitro*.

The cytotoxicity and oxidative stress caused by 5-nm $CeO_2$ nanoparticles in cultured human melanoma cells (A375) were investigated. Concentrations of CNP being nontoxic on stromal cells (*e.g.,* fibroblasts and endothelial cells) showed significantly decreased cell viability in tumor cells as a function of nanoparticle concentration and exposure time. Indicators

of oxidative stress and apoptosis, including total ROS, carbonylated proteins, poly(ADP-ribose)polymerase (PARP) cleavage, and caspase-3 activity, were quantitatively assessed. It is concluded from the data that free oxygen radicals generated by $CeO_2$ nanoparticles produce significant oxidative stress in tumor cells, resulting in a decrease in cell viability and lowering of the invasive capacity of cancer cells.

### *Characterization and cellular uptake of CNP*

The characteristics of nanoparticles such as size and shape are crucial for determining their functional role in tumor cells. Therefore, the synthesized particles were examined using high-resolution transmission electron microscopy (HRTEM) to determine particle size [Supplementary Fig. S1A(a); Supplementary Data are available online at www.liebertpub.com/ars]. The micrographs show an individual particle size of $\sim$5 nm and depicting lattice fringes of CNP with a 0.31-nm selected area electron diffraction pattern showing fluorite structure [Supplementary Fig. S1A(b)].

Both, the coated and noncoated samples have a mixed valance state of $Ce^{3+}$ and $Ce^{4+}$ on the surface with a stable predominance of 4+ oxidation state for coated samples (ratio $Ce^{3+}/Ce^{4+} = 21/79$) and a predominance of 3+ for noncoated samples (ratio $Ce^{3+}/Ce^{4+} = 67/33$) (Supplementary Fig. S1B) measured and calculated by X-ray spectroscopy. As for the proposed SOD mimetic activity of CNPs (31), a higher percentage of $Ce^{3+}$ is needed. For the subordinated catalase-mimetic activity (3, 44), the lower percentage of $Ce^{3+}$ of the coated particles is sufficient (Supplementary Fig. S2C,D).

In addition, a slow reduction of freshly synthesized noncoated CNPs upon aging in water for 7 days was confirmed earlier (3), reflecting a change in the ratio of $Ce^{4+}/Ce^{3+}$ toward $Ce^{3+}$. The aging of nanoparticles in dextran does not reduce CNPs to the same extent as the noncoated CNPs after 7 days of aging, indicating a stable $Ce^{4+}/Ce^{3+}$ ratio toward $Ce^{4+}$ at a neutral pH.

Moreover, the dextran-coated nanoparticles have an added advantage of stability in alkaline to the neutral medium in contrast to noncoated particles that are stable in an acidic medium only. Another significant advantage by coating these particles with dextran is that the individual nanoparticles are of the size 3–5 nm and do not agglomerate in suspension (Supplementary Fig. S2A). HRTEM indicated no agglomeration tendency over a period of 3 months (data not shown). Taken together, the stable dextran-coated CNPs were used for further studies.

A human melanoma cell line (A375) was used to demonstrate the cellular uptake of the particles. Cells were treated with fluorescein isothiocyanate (FITC)-labeled CNPs for 4 h and, thereafter, prepared for visualization. The CNPs were ubiquitously distributed in the cytosol [Supplementary Fig. S1C(b)] compared with the mock-treated control (a). TEM was used to confirm the presence of nanoceria in A375 cells as well. The TEM micrographs of human melanoma cells show $CeO_2$ nanoparticles at 1 h upon treatment as solid black dots localized in the cytosol [Supplementary Fig. S1C(d)].

### *Effect of CNP on tumor growth and angiogenesis* in vivo

To investigate the effect of CNP on human malignant melanoma growth, A375 cells were injected subcutaneously to the flank of nude mice to initiate tumor development *in vivo*. Group 1 of six mice were untreated; group 2 was treated with CNPs starting with day 1 post-tumor cell injection; and the last set (group 3) of tumor-cell-injected mice was treated with CNPs starting with day 10 after injection. The CNP was injected intraperitoneally every alternate day. After dissection of tumors from mice after 30 days postinjection of tumor cells, a significant lowered tumor growth was observed for both applications of CNPs (Fig. 2A). In contrast to mock-treated controls, a significant smaller tumor volume of about 75% (1 d) and 85% (10 d) was determined after CNP treatment (Fig. 2B). Furthermore, the tumor weight was significantly reduced for both CNP applications of about 70% compared with mock-treated tumor-bearing mice (Fig. 2C), indicating a positive effect of CNP on inhibition of malignant melanoma growth *in vivo*. At first view, it seemed not clear that why there was no significant difference between a treatment with CNP starting at day 1 (1 d) or day 10 (10 d) postinjection of tumor cells. However, it depended on the experimental approach and on a delay in the initial growth of the injected tumor cells. After a delay of growth in the order of 10 to 14 days showing some small nodules only, the growth of tumor cells not treated with CNP dramatically increased for the rest of the studied time period in contrast to CNP-treated tumor cells. Therefore, the treatment with CNP starting at 1 or 10 days after tumor cell injection did not show a significant difference having a look on tumor volume or weight.

These data show for the first time in an *in vivo* model that CNP may have the potential as an anticancer agent. In that context earlier, published data show an alternate effect on stromal cells, indicating the dual role of CNP, protective on stromal cells, and damaging on tumor cells (2).

As many studies implicate tumor-associated blood vessel formation as a central part in the process of growth, invasion, and metastasis of malignancies (50), angiogenesis and tumor-associated neovascularization are complex processes by which new blood vessels are formed from pre-existing vasculature. To examine the effect of CNP on angiogenesis *in vivo*, each tumor was subjected to immunohistological analysis of CD31 (PECAM-1). CNP treatment starting with day 1 and 10 after tumor cell injection in nude mice significantly lowered ($\sim$60%) CD31 in the tumor sections compared with the control group (Fig. 2D). These data indicate an inhibiting effect of CNP on migration of endothelial cells in the context to neovascularization, which correlates with a lowered invasive capacity of CNP-treated endothelial cells in an *in vitro* Matrigel assay (Supplementary Fig. S3). The most widely used endothelial cell marker for studying angiogenesis/neovascularization is, for example, CD31 (PECAM-1). CD31 is strongly expressed by all endothelial cells and weakly expressed by several types of leukocytes (43). Staining of blood vessels with CD31 antibodies has been shown to be suitable for the identification of angiogenesis in several types of malignancies (23). According to the literature, the density and morphological state of microvessels in a tumor are closely correlated with prognosis and biological behavior. Therefore, CNP can be considered as promising antitumor agent.

On the basis of the promising results with the xenograft model, we performed a set of *in vitro* experiments to get insight into the underlying molecular mechanism modulated by CNP in melanoma.

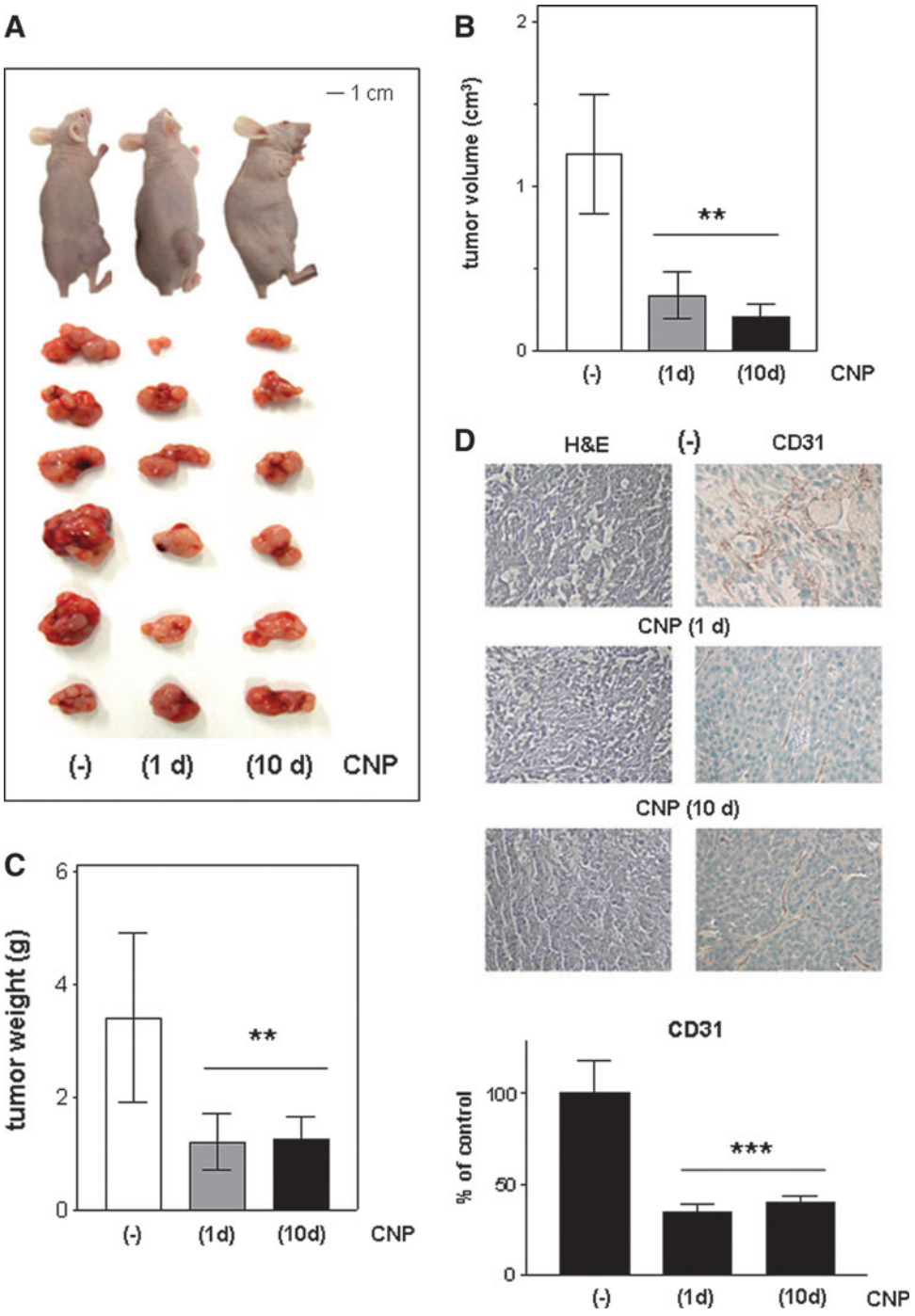


**FIG. 2. Inhibitory effect of CNP on the growth of A375 xenografted mice. (A)** Images of dissected tumors. Three groups of mice were used. Group 1 is vehicle-treated [mock-treated, (−)]; group 2 is CNP-treated starting with day 1 after tumor injection; and group 3 is CNP-treated starting with day 10 after tumor injection. After 30 days, the tumors were dissected. **(B)** Tumor volume. The tumor volume of six mice per group was measured. $^{**}p < 0.01$ *versus* ct (ANOVA and Dunnett's test). Data are presented as means ± SD. **(C)** Tumor weight. The tumor weight of six mice per group was measured. $^{**}p < 0.01$ *versus* ct (ANOVA and Dunnett's test). Data are presented as means ± SD. **(D)** H&E and CD31 staining. Formalin-fixed tissues were embedded in paraffin and sectioned for immunohistological analysis of angiogenesis via CD31 staining and H&E staining for morphology. The percentage of CD31 staining is presented. $^{***}p < 0.001$ *versus* ct (ANOVA and Dunnett's test). Data are presented as means ± SEM.

*Effect of CNPs on cell proliferation*

To examine a potential toxic effect of CNP, melanoma cells were incubated with 5-nm-sized nanoparticles for 96 h. The cell proliferation was analyzed by MTT assays. As shown in Figure 3A, cell viability of A375 cells was decreased by treatment with 150 $\mu M$ nanoceria for 96 h. A concentration of 150 $\mu M$ CNP was used, which was shown earlier (3) to be nontoxic for normal cells, but having a cytotoxic effect on squamous carcinoma cells. The cytotoxicity of polymer-coated CNPs on stromal cells (human dermal fibroblasts [HDFs] and human microvascular endothelial cells [HMEC-1]) was compared with melanoma cells (Fig. 3A). The viability of normal cells was evidently not altered at 96 h after treatment with CNP, whereas melanoma cells showed a lowering of the viability by around 45%. However, no change of cell viability was observed for the three different cell types after treatment with dextran only (mock-treated) compared with untreated controls (ct). These results suggest that the cytotoxic effect of the dextran-coated nanoparticles depends on the redox-active $CeO_2$ and is not affected by the polymer. Those coated CNPs possess great selectivity between cancer and normal cells, and they display potential application in melanoma chemoprevention. In that context, the cytotoxic

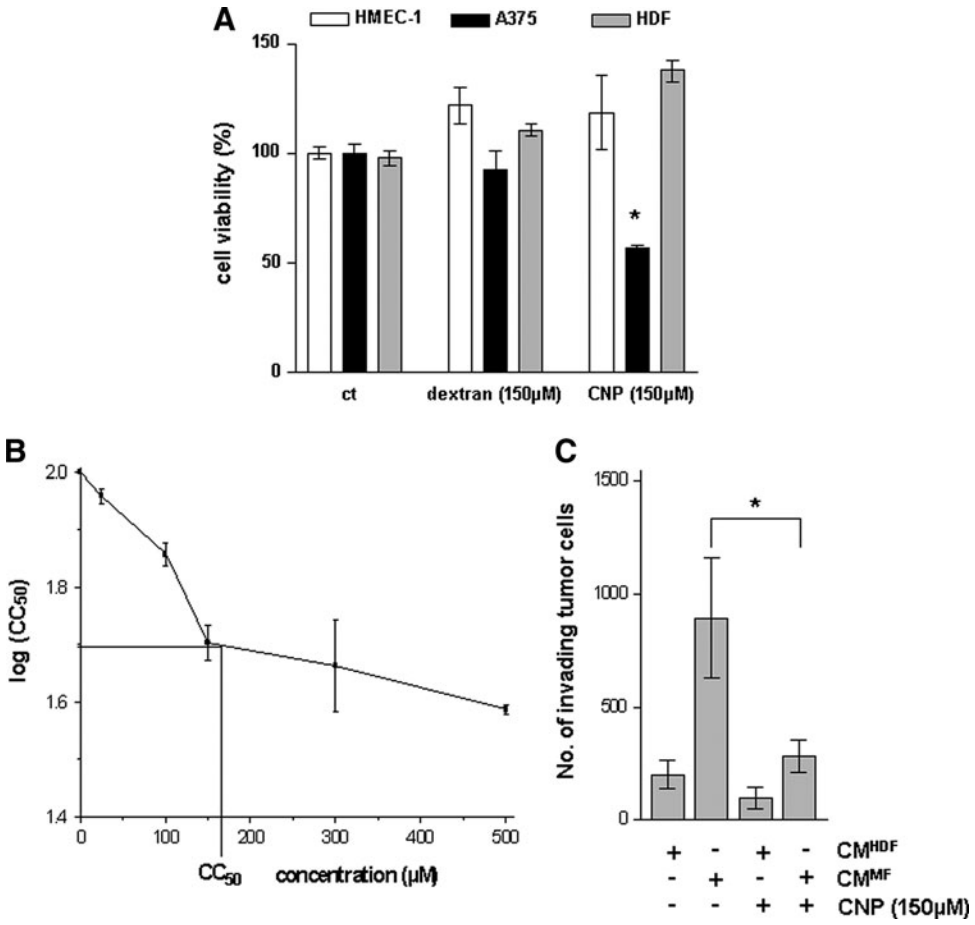


**FIG. 3. Increased cytotoxicity and decreased invasion in CNP-treated tumor cells. (A)** Cytotoxicity of cerium oxide ($CeO_2$) on normal and melanoma cells. Subconfluent melanoma cells (A375), HDFs, and human microvascular endothelial cells (HMEC-1) were treated with CNP or with dextran only (mock-treated) or untreated (ct). The percentage of living cells after 96 h was measured by MTT assay. The experiments were performed in two independent experiments with triplicates in each group. $^*p < 0.05$ *versus* ct (Student's *t*-test). **(B)** The $CC_{50}$ value against melanoma cells. Subconfluent melanoma cells (A375) were treated with various concentrations of CNP. The percentage of living cells after 96 h was measured by MTT assay. The experiments were performed in three independent experiments. **(C)** Anti-invasive impact of CNP on melanoma cells. Subconfluent melanoma cells (A375) were treated with CNP or mock-treated before used for invasion assays. The invasive capacity of these cells was tested with a conditioned medium of HDFs ($CM^{HDF}$) and myofibroblasts ($CM^{MF}$). The data represent the mean ± standard error of the mean (SEM) of three independent experiments. $^*p < 0.05$ *versus* $CM^{MF}$ (Student's *t*-test).

concentration values that cause destruction in 50% of the proliferating cells ($CC_{50}$) were determined being 166 $\mu M$ for melanoma cells, and no toxicity was observed for CNP concentrations up to 1 m*M* for fibroblasts and for the studied endothelial cells. That data indicate a higher sensitivity of melanoma cells against the polymer-coated nanoparticles (Fig. 3B).

### *Involvement of CNP in tumor invasion*

As αSMA-expressing myofibroblasts (MF), often found at the invasion front of many tumors (13), increase the invasive capacity of tumor cells (10), the potential of CNP to prevent invasion on melanoma cells was studied using the conditioned medium (CM) of myofibroblasts ($CM^{MF}$) and normal fibroblasts ($CM^{HDF}$), which were used as control. Therefore, A375 melanoma cells were incubated with different concentrations of CNP. Forty-eight hours after treatment, the invasive capacity of these cells and mock-treated control cells was tested with $CM^{HDF}$ and $CM^{MF}$ (Fig. 3C). Indeed, the invasive capacity of tumor cells is modulated by CNP. Compared to mock-treated tumor cells, the invasive capacity of CNP-treated A375 cells was significantly lowered by 70% using both, $CM^{HDF}$ and $CM^{MF}$.

### *Modulation of ROS generation and protein oxidation by CNP*

To study a possible effect of nanoceria-initiated ROS on toxicity and invasion of tumor cells, we assessed ROS generation both intracellularly and extracellularly. The intracellular ROS level of HDFs was compared with the ROS level of A375 melanoma cells. The treatment of both HDFs and melanoma cells resulted in a significant twofold increase in the ROS level in the tumor cells, whereas no increase was detected in the fibroblasts. Interestingly, the treatment of both cell types with the chemotherapeutical ROS-producing drug doxorubicin (14, 45), which was used as control, significantly increased the intracellular ROS level in both cell types (Fig. 4A). These data

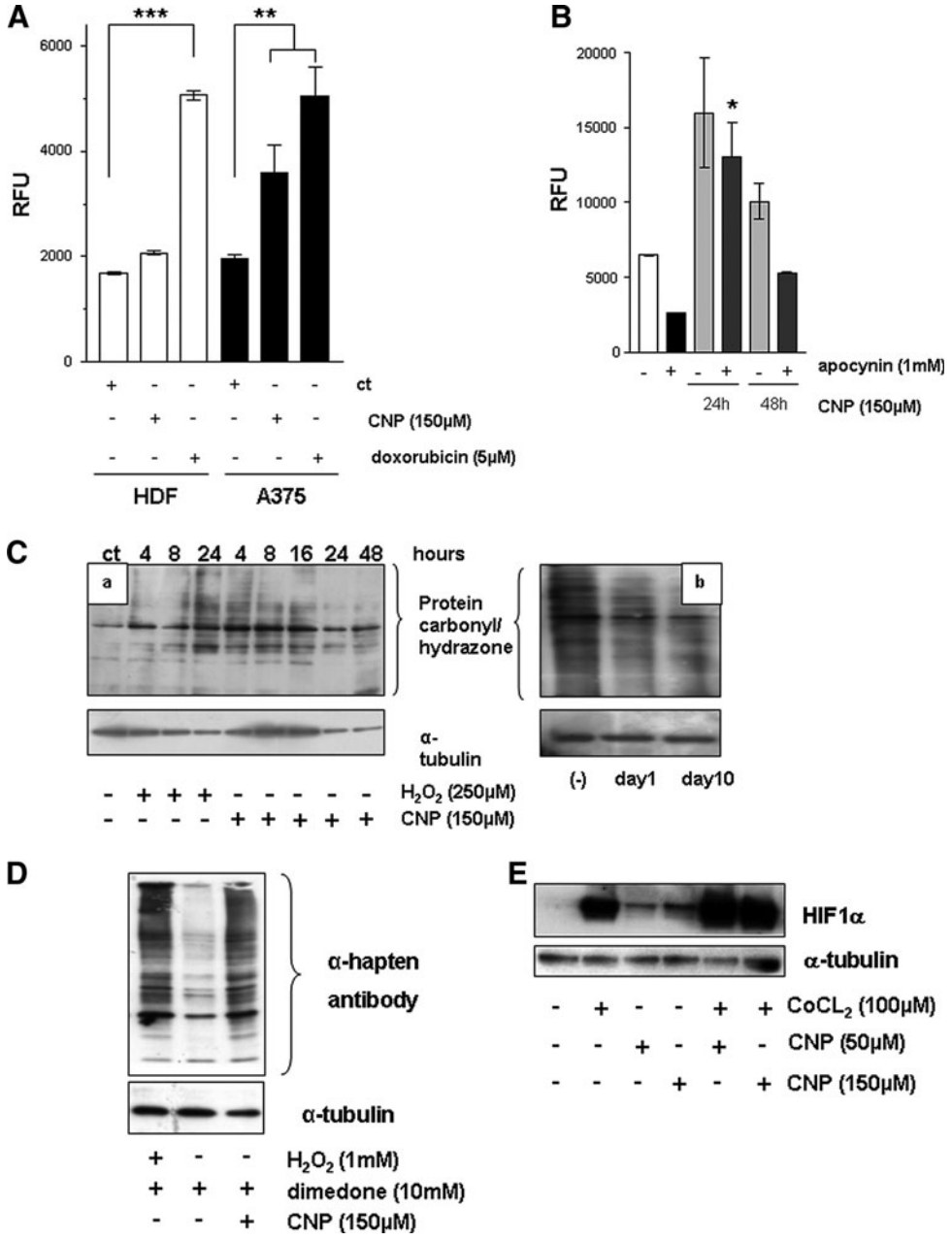


**FIG. 4. Increased reactive oxygen species (ROS) level and oxidative damage in $CeO_2$-treated tumor cells. (A)** Intracellular generation of ROS by CNP. Subconfluent A375 and HDFs were serum-starved for 24 h. The cells were incubated with DCF for 30 min and then mock-treated, CNP-, or doxorubicin treated. The increase in DCF fluorescence as a measure of increase in ROS was followed over 90 min. Results are representative for two independent experiments with triplicates in each group. **(B)** Pro-oxidant effect of CNP. Hydrogen peroxide ($H_2O_2$) was detected using the Amplex Red reagent. The data represent the mean ± SEM of three independent experiments. *$p < 0.05$ *versus* ct (ANOVA and Dunnett's test). **(C)** Detection of CNP-induced carbonylated proteins *in vitro* and *in vivo*; A375 cells were exposed to CNP for different time intervals before oxidized proteins were detected by western blot analysis via derivatisation with 2,4-dinitrophenyl hydrazine. $H_2O_2$ was used as positive control and α-tubulin as loading control **(a)**. Three independent experiments were performed. Protein lysates prepared from flash-frozen tissues of the xenograft mouse model were used in western blot procedures to assess generalized protein oxidation **(b)**. **(D)** Profiling sulfenic acid modifications in A375 cells. Protein was isolated from cells incubated in a medium containing dimedone, in combination with $H_2O_2$ for 2 h or CNP for 24 h. Sulfenic acid-modified proteins were analyzed by western blot with the α-hapten antibody. α-tubulin was used as loading control. Three independent experiments were performed. **(E)** CNP treatment leads to ROS-dependent accumulation of hypoxia-inducible factor 1 alpha (HIF1α). A375 cells were treated with CNP for 24 h. Cobalt chloride ($CoCl_2$), a hydroxylase inhibitor, was added for the last 4 h. The amount of HIF1α protein was determined by western blot analysis. α-tubulin was used as loading control. Three independent experiments were performed.

suggest a pro-oxidant effect of CNP in tumor cells and a different sensitivity of tumor cells against CNP compared with normal cells that could be a benefit of such nanoparticles in the context of future therapeutical approaches. As CNP treatment resulted in an intracellular increase in ROS in tumor cells, a potential extracellular increase in hydrogen peroxide ($H_2O_2$) should be measured with the chemically stable fluorogenic probe *N*-acetyl-3,7-dihydroxyphenoxazine (Amplex Red), which is highly sensitive for the determination of extracellular $H_2O_2$ (66).

CNP exposure resulted in a significant increase in peroxide generation (Fig. 4B). A maximum of the $H_2O_2$ level was measured 24 h after treatment of A375 melanoma cells with CNP, which resulted in a 2.3-fold higher $H_2O_2$ amount compared to mock-treated controls. A decrease of the $H_2O_2$ amount was observed between 24 and 48 h. Melanoma cells treated for 48 h with CNP resulted in an up to a 1.6-fold higher $H_2O_2$ level compared to mock-treated control. As the production of $H_2O_2$ by CNP needs a superoxide source (31), the effect of apocynin on the production of $H_2O_2$ was measured. Apocynin, a methoxy-substituted catechol, inhibits NAD(P)H oxidase by impeding the assembly of p47phox and p67phox subunits within the membrane NAD(P)H oxidase complex (54). Preincubation of melanoma cells for 1 h with apocynin before CNP treatment downregulated the CNP-mediated $H_2O_2$ generation, both at 24 and 48 h. However, it is evident that CNP exposure results in a solid generation of $H_2O_2$.

Another, a more indirect, approach to measure the intracellular generation of ROS and the occurrence of carbonylated proteins, a biomarker for intracellular oxidative stress, was detected. For that, A375 melanoma cells were treated with CNP for 4–48 h and the carbonylated proteins verified. A low amount of carbonylated proteins was detected in mock-treated A375 cells, whereas the amount was significantly increased in $H_2O_2$- and CNP-treated cells compared to mock-treated cells after all studied time points [Fig. 4C(a)]. However, the highest amount of carbonylated proteins was detected at 4 h post-treatment with CNP with a stepwise lowering of the amount between 8 and 48 h [Fig. 4C(a)]. Furthermore, protein lysates prepared from flash-frozen tissues were used in western blot procedures to assess carbonylation of proteins in tumor of mice. A high amount of carbonylated proteins was detected in tumors of mice, which were not treated with CNPs [Fig. 4C(b)]. CNP treatment starting at day 1 and 10 after tumor cell injection in nude mice and finished 30 days postinjection lowered the amount of carbonylated proteins in the tumor lysates, compared to untreated mice. That lowered amount of oxidized proteins in CNP-treated mice correlates with the cell culture data [Fig. 4C(a)] and is due to the time-dependent cytotoxic cell-killing effect of CNP. In other words, a decrease in the cell number results in a decrease of oxidized proteins. Even though the occurrence of protein carbonyls offers a first hint for CNP-initiated oxidative stress, the measurement of those carbonyls is rather a general measure of an alteration of the cellular redox status. Therefore, a more specific approach, namely, the detection of oxidized thiol (-SOH) groups by $H_2O_2$ (= sulfenic acids), was used to measure a change in the intracellular redox status. The application of an α-hapten antibody directed against sulfenic acid of oxidized protein/peptide residues (51) showed a significant increase in oxidized thiols at 24 h after treatment with CNP compared to the diketone dimedone-treated controls. In addition, treatment of the cells with exogenously added $H_2O_2$ resulted in a similar level of oxidized thiol groups (Fig. 4D).

A further parameter for testing the pro-oxidant status of cells is the accumulated translocation of the hypoxia-inducible factor 1 alpha (HIF1a) to the nucleus (30) and the expression of HIF1α target genes, including proangiogenic factors and enzymes favoring a significant glycolytic metabolism (5, 48). Chemical inhibitors of the prolyl hydroxylase, such as cobalt chloride ($CoCl_2$), inhibit HIF1α degradation and lead to its stabilization, therefore enhancing its detection (42). Treatment of A375 cells with a nontoxic concentration of 100 $\mu M$ $CoCl_2$ for 4 h resulted in a significant stability of HIF1α protein levels (Fig. 4E). Treatment with either 50 or 150 $\mu M$ polymer-coated CNPs for 24 h led to an increase in HIF1α protein expression compared with untreated control. Coincubation of CNP and $CoCl_2$ for 4 h showed an increased HIF1α protein level, which was significantly higher than in the $CoCl_2$-treated controls.

As HIF1α positively affects the expression of glycolytic enzymes resulting, for example, in a higher intracellular lactate and $H^+$ production with a subsequent decrease of the microenvironmental pH of tumor cells (22, 57), the question was addressed of whether the pro-oxidant effect of CNP on tumor cells may due to a higher lactate/$H^+$ production of these cells *versus* (stromal) fibroblasts. Indeed, the A375 melanoma cells produced up to 38% more lactate compared to the fibroblasts (Supplementary Fig. S4). This increase in the lactate and $H^+$ level explains the SOD-mimetic activity of nanoceria [(a) $Ce^{4+} + O_2\bullet^- \rightarrow Ce^{3+} + O_2$, (b) $Ce^{3+} + 2H^+ + O_2\bullet^- \rightarrow Ce^{4+} + H_2O_2$)], which was published earlier (3, 31).

The CNP-mediated increase in the intracellular ROS level allows the conclusion that the change of the intracellular redox status in tumor cells may play an important role in the increased cellular toxicity and lowering of the invasive capacity. This hypothesis was checked in subsequent experiments.

### *Induction of apoptosis by CNP*

To assess whether the cytotoxic effect of polymer-coated CNPs in melanoma cells was caused by ROS-mediated apoptotic cell death, the occurrence of apoptotic biomarkers such as cytochrome c release, caspase-3, and PARP cleavage was measured.

The release of cytochrome c is an early event of the intrinsic apoptotic cascade initiated, for example, by ROS (29). In that context, treatment of the melanoma cells with $H_2O_2$ for 1 h resulted in a significant increase of cytosolic cytochrome c compared to mock-treated controls. A similar elevated level of cytosolic cytochrome c was detected after treatment of the tumor cells with CNP for 12 and 24 h (Fig. 5A). The CNP treatment resulted in a 6.1-fold increase. As illustrated in Figure 5B, the activity of caspase-3 was significantly increased by CNP in A375 cells compared to mock-treated control cells. At 24 h post-treatment with CNP, an up to 1.9-fold increase in the caspase-3 activity was measured. Furthermore, the natural material staurosporine, which induces caspase-3 activity in melanoma cells (39), and which was used herein as positive control, increased the activity of caspase-3.

In addition to the cytochrome c release and caspase-3 activity assay, PARP cleavage was evaluated. Caspase

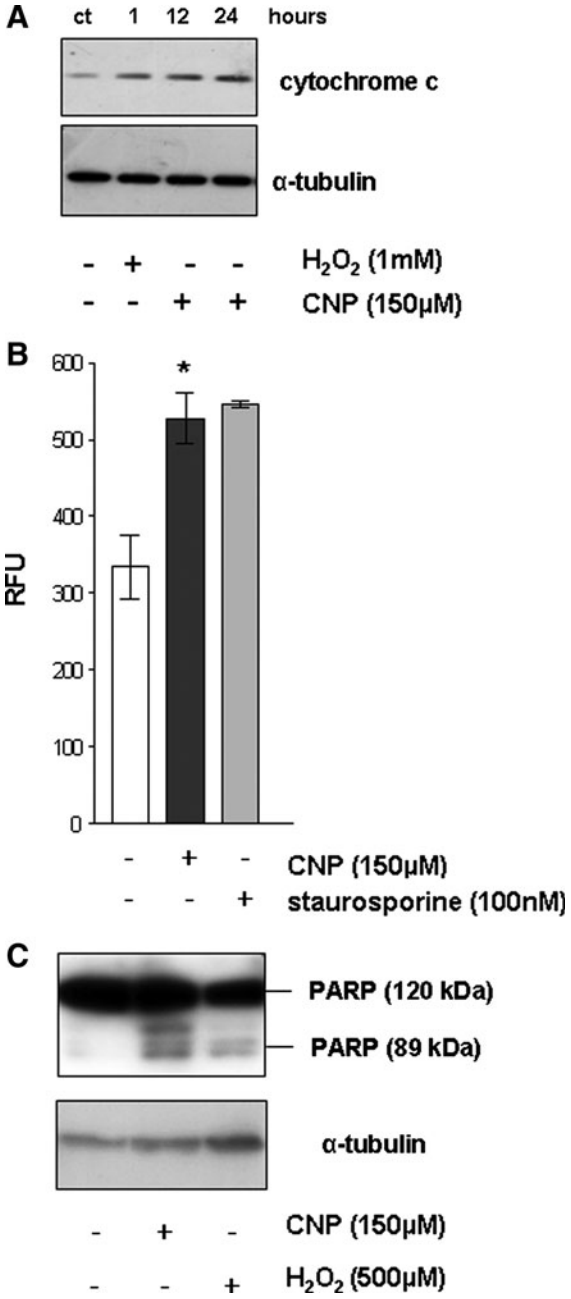


**FIG. 5. CNP treatment caused apoptosis in A375 cells. (A)** Subcellular distribution of cytochrome c. Subconfluent A375 cells were either mock-treated or incubated for 12 and 24 h; CNP and cytochrome c levels were determined by western blot in the cytosolic fraction. $H_2O_2$ was used as positive control and α-tubulin as a loading control. Three independent experiments were performed. **(B)** Increased Caspase-3 activity in melanoma cells. Caspase-3 activity was measured using a fluorometric caspase-specific substrate (Ac-DEVD-AMC). Staurosporine was used as positive control. Results represent the means of three separate experiments, and error bars represent SEM. Statistical significance was shown by the Student's *t*-test *versus* ct (*$p < 0.05$). **(C)** Cleavage of poly(ADP-ribose) polymerase (PARP). Representative western blot shows PARP cleavage after incubation of melanoma cells for 24 h with CNP compared to mock-treated control (ct). $H_2O_2$ was used as positive control and α-tubulin as loading control. Three independent experiments were performed.

activation subsequently induces proteolytic cleavage of PARP, which serves as a biochemical marker of cells undergoing apoptosis (8). CNP treatment for 24 h induced PARP cleavage in melanoma cells compared to mock-treated control, which was demonstrated by the appearance of the 89-kDa fragment (Fig. 5C). Treatment of the tumor cells with exogenously added $H_2O_2$ resulted in PARP cleavage as well. Apoptosis is initiated by two central mechanisms, the extrinsic (36) and intrinsic pathway (41). Exposure of A375 cells to CNP resulted in cytochrome c release, activation of caspase-3, and PARP cleavage (Fig. 5A–C), which indicated the activation of the intrinsic pathway of apoptosis. In that context, it is described that gold nanoparticles (AuNPs) resulted in a significant increase in $H_2O_2$ generation, and thus apoptosis is irreversibly induced (17). In conclusion, CNPs lead to a pro-oxidant status of the tumor cells resulting in proapoptotic mechanism.

### *Caveolin-1 downregulation by CNP*

The role of ROS in the cellular invasion and migration was described earlier (34, 55). Caveolin-1 (Cav-1) has received the most attention, since its expression has been linked to cancer progression and aggressiveness (58). Cav-1 plays a role not only in cell death and survival, but also in cell migration (38) and invasion (61). It is consistent that both $H_2O_2$ and superoxide ($O_2^{\bullet -}$) have an inhibitory effect on expression of Cav-1, while hydroxyl radicals increase Cav-1 expression and migration (38). Melanoma cells were treated with CNP for 1 h, and Cav-1 expression was detected. CNP caused a significant downregulation of Cav-1 expression compared to the mock-treated control (Fig. 6). Incubation of the cells with exogenous $H_2O_2$ for 1 and 4 h completely abrogated Cav-1 expression. By contrast, pretreatment of melanoma cells with the antioxidant N-acetyl-L-cysteine or apocynin resulted in an increased Cav-1 expression compared to CNP-treated cells. These data indicate the involvement of CNP-initiated ROS in lowering the invasive capacity of the studied tumor cells.

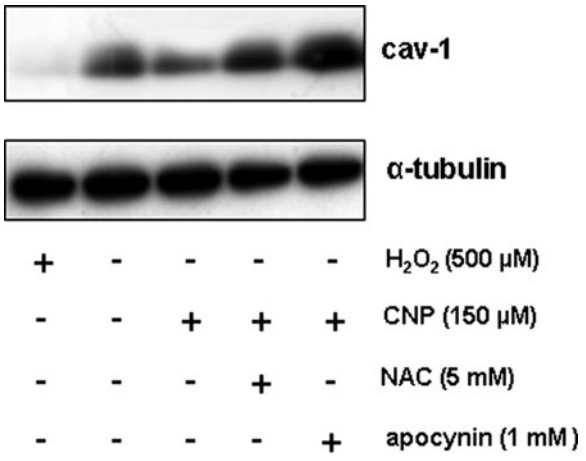


**FIG. 6. Expression of caveolin-1 (Cav-1) in melanoma cells.** Representative western blot demonstrates Cav-1 protein expression in A375 cells mock-treated, CNP treated for 24 h, or preincubated with apocynin for 1 h or *N*-acetyl-L-cysteine for 4 h, and then CNP treated for 24 h. $H_2O_2$ was used as a positive control and α-tubulin as a loading control. Three independent experiments were performed.

## Discussion

As both the incidence of melanoma is increasing faster than that of other cancers and the chemotherapeutical treatment of a majority of patients with metastatic melanoma often results in adverse reactions and response rates that are not high enough to significantly affect median survival, novel therapeutical approaches should be the objective for the near future. In this study, we have shown for the first time *in vitro* and *in vivo* that concentrations of polymer-coated CNPs being nontoxic for stromal cells exhibit a direct ROS-dependent cytotoxic (proapoptotic) and anti-invasive effect on melanoma cells. Our study highlights a prospective clinical significance of polymer-coated CNPs.

Recently, a number of studies have focused on the interaction between nanoparticles and biological systems to evaluate novel strategies for an efficient drug delivery and possible alternative cancer therapies. Magnetic iron nanoparticles, for example, are used in cancer therapy. Cancer cells incubated with these particles and then magnetically heated show decreased viability, whereas normal cells remain unaffected (32). Polymer-coated CNPs with a size of ø20 nm and in higher concentrations then used herein generate free oxygen species in human lung cancer cells and produce significant oxidative stress and subsequent decrease in the cell viability (37). However, the effect of that high concentration of CNP on normal (stromal) cells was not studied. We described earlier that CNPs with a smaller size and lower concentration result in an antioxidant and protective effect in (stromal) fibroblasts (3). CNPs (nanoceria) have a unique electronic structure that is mediated by their large surface-area-to-volume ratio (28), resulting in valance and oxygen defects on the surface of that particles. Therefore, nanoceria possess a promising pharmacological potential, suggesting that nanoceria may be used as an antioxidant agent (11). The antioxidant ability is associated with the SOD-mimetic (21, 31) and catalase-mimetic activities (44) of nanoceria that were measured primarily in a cell-free system. Recently, we published an antioxidative activity of CNPs in normal cells and, surprisingly, a pro-oxidant effect in cells of a squamous skin tumor (3). In that context, the data presented herein with melanoma cells support a pro-oxidant (SOD-mimetic) mechanism of nanoceria that depends on the pH of the cells. As a higher lactate/$H^+$ production was detected in A375 cells (see Supplementary Fig. S3), the following chemical mechanisms are suggested: (a) $Ce^{4+} + O_2{\bullet}^- \rightarrow Ce^{3+} + O_2$ and (b) $Ce^{3+} + 2H^+ + O_2{\bullet}^- \rightarrow Ce^{4+} + H_2O_2$). As Figure 4A and B indicate a production of superoxide and an increase in $H_2O_2$ in the melanoma cells and Supplementary Figure S1B shows a higher percentage of $Ce^{4+}$ in coated nanoparticles, which is important for the initial SOD-mimetic mechanism, these results in accordance with earlier published data support the proposed pro-oxidant effect of polymer-coated CNPs. That pro-oxidant effect results in cytotoxicity and decrease of the invasive capacity of the tumor cells.

## Materials and Methods

The cell culture medium (Dulbecco's modified Eagle's medium [DMEM]) was purchased from Invitrogen, and the defined fetal calf serum (FCS gold) was from PAA Laboratories. All chemicals, including protease as well as phosphatase inhibitor cocktail 1 and 2, were obtained from Sigma or Merck Biosciences unless otherwise stated. The protein assay kit (Bio-Rad DC; detergent-compatible) was from BioRad Laboratories. Matrigel and polycarbonate cell culture inserts (6.5-mm diameter; 8-$\mu$m pore size) were delivered from BD Biosciences. The Oxyblot Protein Oxidation Detection kit was from Millipore, whereas the Amplex Red Hydrogen Peroxide/Peroxidase Assay Kit was provided from Invitrogen. The enhanced chemiluminescence system (SuperSignal West Pico/Femto Maximum Sensitivity Substrate) was supplied by Pierce. Monoclonal mouse antibody raised against human αSMA and α-tubulin was supplied by Sigma. Polyclonal rabbit antibody raised against human HIF1α and Cav-1 was supplied by New England Biolabs. The polyclonal rabbit α-hapten antibody directed against oxidized thiol groups (sulfenic acid) (50) was a gift from Kate S. Carrol's group. The following secondary antibodies were used: polyclonal horseradish peroxidase (HRP)-conjugated rabbit anti-mouse IgG antibody (Dako) and goat anti-rabbit immunoglobulin G antibodies, which were from Dianova. Recombinant human TGF$\beta$1 (rTGF$\beta$1) was from R&D Systems.

### *Cell culture*

HDFs were established by outgrowth from foreskin biopsies of healthy human donors with an age of 3–6 years. Cells were used in passages 2–12, corresponding to cumulative population-doubling levels of 3–27 (6). The human malignant melanoma cell line A375, originally derived from a 54-year-old woman, was purchased from ATCC (20). The immortalized HMEC-1, which expresses cell surface molecules typically associated with primary endothelial cells, was obtained from the Centers for Disease Control (1). Dermal fibroblasts, melanoma, and endothelial cells were cultured as described (56). MF were generated by treatment of HDFs with rTGF$\beta$1 for 48 h in $CM^{HDF}$ (10).

### *Preparation of CM*

The CM was obtained from HDFs ($CM^{HDF}$) and myofibroblasts ($CM^{MF}$). For this, seeded $1.5 \times 10^6$ HDFs were grown to subconfluence ($\sim$70% confluence) in 175-$cm^2$ culture flasks. The serum-containing medium was removed, and after washing in phosphate-buffered saline (PBS), the cells were treated with 5 ng/ml or without rTGF$\beta$1 in a serum-free DMEM for 48 h. This medium was removed, and after washing in PBS, all cells were incubated in 15 ml serum-free DMEM for further 48 h before collection of the $CM^{HDF}$ and $CM^{MF}$. The CM was freshly used or stored at $-20$°C for at the most 2 weeks before use.

### *Cell viability*

The cytotoxic effect of CNPs was measured by MTT [3-(4, 5-Dimethylthiazol-2-yl)-2,5-diphenyltetrazolium bromide] assay (40). The activity of mitochondrial dehydrogenases, as indicator of cellular viability, results in the formation of a purple formazan dye. Briefly, the MTT solution (0.5 mg/ml) was added to the cells treated with different concentrations of CNPs for 96 h after washing with PBS. The medium was removed, and the cells were lysed in dimethyl sulfoxide. The formazan formation was measured at 570 nm. The results were presented as a percentage of mock-treated control, which was set at 100%. The $CC_{50}$ value was defined as the concentration that reduced the absorbance of treated cells to 50% when compared to mock-treated (control) cells.

### Synthesis of CNPs

CNPs were synthesized in dextran (molecular weight: 1000 Da) using previously described methods (26). Briefly, cerium nitrate hexahydrate was dissolved in deionized water, and the pH of the solution was maintained between 3.5 and 4.0 for uncoated (water-based) nanoparticles. Stoichiometric amounts of $H_2O_2$ and ammonium hydroxide were added to oxidize the dissolved cerium ions as CNPs. The pH of the solution needs to be maintained strictly below 4.0 to avoid precipitation of the nanoparticles. For synthesis of dextran-coated nanoparticles, a stoichiometric amount of dextran (5 m*M*) was at first dissolved in deionized water (18.2 MΩ) followed by cerium nitrate hexahydrate. The solution was stirred for 2 h followed by addition of ammonium hydroxide (30% w/w) to oxidize the dissolved cerium ions as CNPs. The pH of the solution was kept below 9.5 to avoid precipitation of cerium hydroxide. The resulting dextran-coated CNPs (nanoceria) were analyzed using UV–Visible spectroscopy for determining the oxidation state of nanoparticles. TEM and dynamic light scattering were used to determine the particle size and hydrodynamic radius of the nanoparticles. Catalase and SOD activity was determined as described in our previous publication (3). After preparation of dex-CNP, we dialyzed the solution to remove excess dextran for 48 h against $dH_2O$ using a 1200-molecular-weight cut-off dialysis membrane, and then Fourier transform infrared spectroscopy (FTIR) was carried out to confirm coating/presence of dextran on the surface of CNP. FTIR data of bare CNP, dextran, and dextran-CNP are shown in Supplementary Figure S5. FTIR data confirm the presence of dextran coating on the surface of the CNP. FTIR spectra were collected to confirm the dextran molecule on the nanoparticle surface using PerkinElmer Lamda750S and PerkinElmer Spectrum.

### High-resolution TEM

High-resolution transmission electron micrographs were obtained using an FEI Tecnai F 30 microscope operated at 300 kV with a point-to-point resolution of 0.2 nm. The samples were prepared by depositing a drop of dextran-coated CNP on a holy carbon-coated copper grid. The grids were dried overnight in vacuum before imaging.

### X-ray spectroscopy

X-ray photoelectron spectroscope (XPS) spectra of Ce(3*d*) were collected using a 5400 PHI ESCA (XPS) spectrometer, and Mg-Kα X-radiation (1253.6 eV) at a power of 350 watts was used during the data collection. $Ce^{4+}/Ce^{3+}$ oxidation state ratio on the surface of bare and dextran-coated CNPs was analyzed by deconvoluting the XPS spectrum of Ce(3*d*), as described elsewhere (12). The peaks at 880.8, 885.8, 899.3, and 903.5 eV corresponding to the $Ce^{3+}$ oxidation state and peaks at 881.9, 888.4, 897.9, 901.2, 906.8, and 916.3 eV corresponding to the $Ce^{4+}$ were assigned. Intensities of the peaks were determined, and the $Ce^{3+}/Ce^{4+}$ ratios calculated.

### Cellular uptake of nanoparticles

Human melanoma cells in a serum-free DMEM were treated with 150 μ*M* CNP for 4 h. Thereafter, cells were harvested and washed with PBS to remove the excess medium. As CNP is not detectable by phase-contrast microscopy, TEM was used to determine the cellular uptake of nanoceria. For electron microscopy, pelleted samples of CNP-treated cells were fixed for 2 h in 4% paraformaldehyde and 2.5% glutaraldehyde (Serva) in 0.1 *M* phosphate buffer at pH 7.4 at room temperature. Next, the pellets were thoroughly washed with four changes of PBS, followed by a postfixation for 60 min in 1% osmium tetroxide (Serva) in PBS. The specimens were dehydrated in a graded series of acetone, and embedded in Spurr's medium (Serva) at 70°C for 24 h. Ultrathin sections were cut from the embedded tissue with a Reichert Ultracut using a diamond knife. The sections were collected on coated copper grids, and subsequently stained with uranyl acetate and lead citrate according to earlier published data (46). The grids were analyzed using a Hitachi H 600 electron microscope. An optical system and Digital Micrograph software (Gatan) were used for documentation. For light-microscopical controls, semithin sections were cut and stained with 1% toluidine blue and 1% borax.

For fluorescence microscopy, cells were incubated with 150 μ*M* FITC-labeled CNPs for 4 h or mock-treated. Thereafter, cells were washed twice with PBS and fixed with methanol. For preparation, ProLong Gold (Invitrogen) was used, a reagent that simultaneously stains the nuclei with DAPI. Zeiss Axiovert 100TV was used for the fluorescence microscopic examination, and a digital camera system (Hamamatsu C4742-95) for documentation.

### Sodium dodecyl sulfate–polyacrylamide gel electrophoresis and western blotting

Sodium dodecyl sulfate–polyacrylamide gel electrophoresis (SDS-PAGE) was performed according to the standard protocols published elsewhere (33) with minor modifications. Briefly, cells were lysed after incubation with CNP in 1% SDS with 1:1000 protease inhibitor cocktail (Sigma). After sonication, the protein concentration was determined by using a modified Lowry method (Bio-Rad DC); 4×SDS-PAGE sample buffer (1.5 *M* Tris–HCl, pH 6.8, 6 ml 20% SDS, 30 ml glycerol, 15 ml β-mercaptoethanol, and 1.8 mg bromophenol blue) was added, and after heating, the samples (20–30 μg total protein/lane) were applied to 8%–15% (w/v) SDS–polyacrylamide gels. After electroblotting, immunodetection was carried out (1:1000 dilution of primary antibodies, rabbit monoclonal anti-αSMA, HIF1α , Cav-1, and mouse monoclonal anti-α-tubulin; and 1:20,000 dilution of anti-mouse/rabbit antibody conjugated to HRP). Antigen–antibody complexes were visualized by an enhanced chemiluminescence system. α-tubulin was used as internal control for equal loading.

### A375 xenograft model of nude mice

One million human melanoma A375 cells ($1\times10^6$) were resuspended in 50 μl PBS, mixed with 200 μl Matrigel (BD Biosciences), and implanted subcutaneously into the right flank of 6–7 weeks old athymic NCr-nu/nu mice from the National Cancer Institute (NCI). The care and experimental manipulation of mice described in this study were in accordance with the guidelines of the Mayo Clinic College of Medicine for the ethical treatment of animals. To distinguish between individual differences in mice, six mice were chosen for each group. Group 1 is vehicle-treated [=mock-treated (0.1 mg dextran/kg body weight)]; group 2 is CNP-treated starting with day 1 after tumor cells were injected; and group

3 is CNP-treated starting with day 10 postinjection of tumor cells. Nanoceria was administered by intraperitoneal injection, every alternate day with the dose of 0.1 mg/kg body weight for 30 days. The day after the last CNP application, the tumor was dissected, and its weight recorded. Three diameters of the tumor ($L$, $B$, and $H$) were measured by a caliper. The volume of the tumor was calculated as $V = \pi/6 \times L \times B \times H$ (62).

### *Immunohistochemistry/histology*

Tumor angiogenesis was assessed by CD31/PECAM-1 (Platelet Endothelial Cell Adhesion Molecule-1) staining of paraffin tissue sections employing a rat monoclonal antibody (Dianova), a biotinylated secondary antibody (Biotin Goat anti-Rat Ig; BD Pharmingen), and streptavidin/peroxidase and diaminobenzidine/$H_2O_2$ (Dako). CD31 staining was quantitated by image analysis using GraphPad Prism software.

### *Measurement of extracellular and intracellular ROS*

The generation of ROS was determined using the Amplex Red Hydrogen Peroxide/Peroxidase Assay Kit. The Amplex Red reagent (10-acetyl-3,7-dihydroxyphenoxine), in combination with HRP, can be used to detect $H_2O_2$ released from cells. $H_2O_2$-mediated oxidation of the reagent results in the fluorescent product resorufin. Subconfluent A375 tumor cells were treated with 150 $\mu M$ CNP or preincubated with 1 m$M$ apocynin in a serum-free DMEM in 96-well plates for different time points. Untreated subconfluent A375 cells were used as negative controls. After incubation with CNP, cells were washed twice with Hank's balanced salt solution (HBSS), and the assay was performed following the manufacturer's instructions. Resorufin fluorescence was detected at an excitation wavelength of 520 nm and emission wavelength of 590 nm in a FLUOstar OPTIMA plate reader (BMG Labtech). Mean fluorescence intensities and standard error of mean (SEM) were determined by using statistical software Prism 3.0 (GraphPad). Furthermore, the generation of intracellular ROS was determined using 2',7'-dichlorodihydrofluorescein diacetate ($H_2$DCF-DA), a dye that diffuses across the lipid membranes into cells and is subsequently oxidized by intracellular ROS forming the highly fluorescent DCF. Untreated subconfluent HDFs and melanoma cells (A375) were used as negative controls. The medium was substituted after 24-h starvation by 100 $\mu M$ $H_2$DCF-DA containing HBSS for 30 min. Subconfluent HDFs and A375 tumor cells were exposed to 150 $\mu M$ CNP and 5 $\mu M$ doxorubicin in the serum-free DMEM in 24-well plates, and DCF fluorescence was detected at an excitation wavelength of 485 nm and emission wavelength of 520 nm in 5-min intervals for 90 min in a FLUOstar OPTIMA plate reader (BMG Labtech). Mean fluorescence intensities and SEM were determined for each reading point by using statistical software Prism 3.0 (GraphPad), and the end point is shown.

### *Determination of oxidized (carbonylated) proteins*

A375 melanoma cells were grown to subconfluence on tissue culture dishes. After removal of the serum-containing medium, cells were cultured in a serum-free medium and either mock-treated or treated for different time periods with 150 $\mu M$ $CeO_2$ nanoparticles. As a positive control, the cells were treated with 250 $\mu M$ $H_2O_2$. Thereafter, cells were lysed and carbonyl groups of oxidized proteins were detected with the OxyBlot™ Protein Oxidation Detection Kit, following the manufacturer's protocol. Briefly, the protein concentration was determined by using a modified Lowry method (Bio-Rad DC). Five $\mu$g of the cell lysates was incubated with 2,4-dinitrophenyl (DNP) hydrazine to form the DNP hydrazone derivatives. Labeled proteins were separated by SDS-PAGE and immunostained using rabbit anti-DNP antiserum (1:500) and goat anti-rabbit IgG conjugated to HRP (1:2000). Blots were developed by enhanced chemiluminescence.

### *Determination of oxidized thiol groups (sulfenic acid)*

A375 melanoma cells were grown to subconfluence on tissue culture dishes. After removal of serum-containing medium, cells were cultured in serum-free medium and either mock-treated or treated for 24 h 150 $\mu M$ $CeO_2$ nanoparticles and the last 2 h with 10 m$M$ dimedone. As positive control, the cells were coincubated with 10 m$M$ dimedone and 1 m$M$ $H_2O_2$ for 2 h. Cells were harvested and washed with PBS, and lysates were generated and analyzed with the α-hapten (1:1000) antibody directed against oxidized –SH groups by western blot analysis.

### *Invasion assay*

Cell culture inserts (transwells) were overlaid with 125$\mu$g/ml growth factor-reduced Matrigel and placed in a 24-well plate. A375 tumor cells ($5 \times 10^4$ cells/insert) either mock-treated or pretreated with 150 $\mu M$ CNP were seeded on top of the Matrigel in a serum-free DMEM. $CM^{HDF}$ and $CM^{MF}$ (see above) were used as chemoattractants in the lower chamber. After 30 h at 37°C, the melanoma cells were rubbed off the upper side of the filter using cotton swabs, and the A375 cells, which invaded toward the lower side of the insert, were stained with Coomassie Blue solution (0.05% Coomassie Blue, 20% MeOH, and 7.5% acetic acid). The number of invaded cells was estimated by counting random microscopic fields/insert.

### *L-lactate assay*

A375 melanoma cells and HDFs were grown to subconfluence on tissue culture dishes. After removal of the serum-containing medium, cells were cultured in a serum-free medium for 24 h. Thereafter, cells were collected by centrifugation (1500 $g$ for 10 min at 4°C). The supernatant was used to quantify extracellular L-lactate with the L-Lactate Assay Kit from Cayman Chemical Company following the manufacturer's protocol.

### *Caspase-3 activity assay*

A375 melanoma cells and HDFs were grown to subconfluence on tissue culture dishes. After removal of the serum-containing medium, cells were cultured in a serum-free medium with 150 $\mu M$ CNP or 100 n$M$ staurosporine for 24 h. Cell pellets were suspended in a cell lysis buffer and incubated on ice for 45 min. The lysate was vortexed every 15 min. After centrifugation at 11000 $g$ for 15 min, supernatants were collected and immediately measured for protein concentration and caspase activity. Briefly, cell lysates (20 $\mu$g protein) were placed in 96-well plates, and then the specific caspase

substrate (Ac-DEVD-AMC for caspase-3) was added. Plates were incubated at 37°C for 1 h, and caspase activity was determined by fluorescence intensity with the excitation and emission wavelengths set at 380 and 440 nm, respectively.

### *Statistical analysis*

Means were calculated from at least three independent experiments, and error bars represent SEM. Analysis of statistical significance was performed by Student's *t*-test or ANOVA with $*p < 0.05$, $**p < 0.01$, and $***p < 0.001$ as levels of significance.

## Acknowledgments

This work is part of the PhD thesis of M.S. at the Heinrich-Heine-University of Düsseldorf. We thank C. Wyrich, V. Pützer, and B. Rohbeck for excellent technical assistance. S. Seal acknowledges the National Science Foundation (NSF) to partially fund the nanotechnology research under NSF NIRT (CBET-0708172) and NSF (CBET-0930170). We would like to thank Candice E. Paulsen and Kate S. Karrol for providing the α-hapten antibody.

## Author Disclosure Statement

The authors declare no competing financial interests.

## References

1. Ades EW, Candal FJ, Swerlick RA, George VG, Summers S, Bosse DC, and Lawley TJ. HMEC-1: establishment of an immortalized human microvascular endothelial cell line. *J Invest Dermatol* 99: 683–690, 1992.
2. Alili L, Karakoti AS, Seal S, and Brenneisen P. Suppression of tumor invasion by inorganic nanoparticles *Cancer Res* 69(23 Suppl.): Boston, C42, 2009.
3. Alili L, Sack M, Karakoti AS, Teuber S, Puschmann K, Hirst SM, Reilly CM, Zanger K, Stahl W, Das S, Seal S, and Brenneisen P. Combined cytotoxic and anti-invasive properties of redox-active nanoparticles in tumor-stroma interactions. *Biomaterials* 32: 2918–2929, 2011.
4. Altekruse SF, KC, Krapcho M, Neyman N, Aminou R, Waldron W, Ruhl J, Howlader N, Tatalovich Z, Cho H, Mariotto A, Eisner MP, Lewis DR, Cronin K, Chen HS, Feuer EJ, Stinchcomb DG, and Edwards BK. *SEER Cancer Statistics Review, 1975–2007*. Bethesda, MD: National Cancer Institute, 2010.
5. Bardos JI and Ashcroft M. Negative and positive regulation of HIF-1: a complex network. *Biochim Biophys Acta* 1755: 107–120, 2005.
6. Bayreuther K, Francz PI, Gogol J, and Kontermann K. Terminal differentiation, aging, apoptosis, and spontaneous transformation in fibroblast stem cell systems *in vivo* and *in vitro*. *Ann N Y Acad Sci* 663: 167–179, 1992.
7. Bhatia S, Tykodi SS, and Thompson JA. Treatment of metastatic melanoma: an overview. *Oncology (Williston Park)* 23: 488–496, 2009.
8. Boulares AH, Yakovlev AG, Ivanova V, Stoica BA, Wang G, Iyer S, and Smulson M. Role of poly(ADP-ribose) polymerase (PARP) cleavage in apoptosis. Caspase 3-resistant PARP mutant increases rates of apoptosis in transfected cells. *J Biol Chem* 274: 22932–22940, 1999.
9. Brenneisen P, Wenk J, Klotz LO, Wlaschek M, Briviba K, Krieg T, Sies H, and Scharffetter-Kochanek K. Central role of ferrous/ferric iron in the ultraviolet B irradiation-mediated signaling pathway leading to increased interstitial collagenase (matrix-degrading metalloprotease (MMP)-1) and stromelysin-1 (MMP-3) mRNA levels in cultured human dermal fibroblasts. *J Biol Chem* 273: 5279–5287, 1998.
10. Cat B, Stuhlmann D, Steinbrenner H, Alili L, Holtkotter O, Sies H, and Brenneisen P. Enhancement of tumor invasion depends on transdifferentiation of skin fibroblasts mediated by reactive oxygen species. *J Cell Sci* 119: 2727–2738, 2006.
11. Celardo I, Traversa E, and Ghibelli. Cerium oxide nanoparticles: a promise for applications in therapy. *J Exp Ther Oncol* 9: 47–51, 2011.
12. Deshpande S, Patil S, Kuchibhatla, SV, and Seal S. Size dependency variation in lattice parameter and valency states in nanocrystalline cerium oxide. *Appl Phys Lett* 87: 133113, 2005.
13. De Wever O and Mareel M. Role of myofibroblasts at the invasion front. *Biol Chem* 383: 55–67, 2002.
14. Fang J, Nakamura H, and Iyer AK. Tumor-targeted induction of oxystress for cancer therapy. *J Drug Target* 15: 475–486, 2007.
15. Freitas RA, Jr. What is nanomedicine? *Nanomedicine* 1: 2–9, 2005.
16. Fruehauf JP and Trapp V. Reactive oxygen species: an Achilles' heel of melanoma? *Expert Rev Anticancer Ther* 8: 1751–1757, 2008.
17. Gao W, Xu K, Ji L, and Tang B. Effect of gold nanoparticles on glutathione depletion-induced hydrogen peroxide generation and apoptosis in HL7702 cells. *Toxicol Lett* 205: 86–95, 2011.
18. Garbe C and Leiter U. Melanoma epidemiology and trends. *Clin Dermatol* 27: 3–9, 2009.
19. Garbe C, Terheyden P, Keilholz U, Kolbl O, and Hauschild A. Treatment of melanoma. *Dtsch Arztebl Int* 105: 845–851, 2008.
20. Giard DJ, Aaronson SA, Todaro GJ, Arnstein P, Kersey JH, Dosik H, and Parks WP. *In vitro* cultivation of human tumors: establishment of cell lines derived from a series of solid tumors. *J Natl Cancer Inst* 51: 1417–1423, 1973.
21. Heckert EG, Karakoti AS, Seal S, and Self WT. The role of cerium redox state in the SOD mimetic activity of nanoceria. *Biomaterials* 29: 2705–2709, 2008.
22. Helmlinger G, Yuan F, Dellian M, and Jain RK. Interstitial pH and pO2 gradients in solid tumors *in vivo*: high-resolution measurements reveal a lack of correlation. *Nat Med* 3: 177–182, 1997.
23. Jahroudi N and Greenberger JS. The role of endothelial cells in tumor invasion and metastasis. *J Neurooncol* 23: 99–108, 1995.
24. Jemal A, Siegel R, Ward E, Hao Y, Xu J, Murray T, and Thun MJ. Cancer statistics, 2008. *CA Cancer J Clin* 58: 71–96, 2008.
25. Kappus H and Sies H. Toxic drug effects associated with oxygen metabolism: redox cycling and lipid peroxidation. *Experientia* 37: 1233–1241, 1981.
26. Karakoti AS, Satyanarayana VN, Kuchibhatla T, Babu KS, and Seal S. Direct synthesis of nanoceria in aqueous polyhydroxyl solutions. *J Phys Chem* C 111: 17232–17240, 2007.
27. Karakoti AS, Monteiro-Riviere NA, Aggarwal R, Davis JP, Narayan RJ, Self WT, McGinnis J, and Seal S. Nanoceria as antioxidant: synthesis and biomedical applications. *Jom* (1989) 60: 33–37, 2008.
28. Karakoti AS, Singh S, Dowding JM, Seal S, and Self WT. Redox-active radical scavenging nanomaterials. *Chem Soc Rev* 39: 4422–4432, 2010.

29. Kawiak A, Zawacka-Pankau J, Wasilewska A, Stasilojc G, Bigda J, and Lojkowska E. Induction of apoptosis in HL-60 cells through the ROS-mediated mitochondrial pathway by Ramentaceone from *Drosera aliciae*. *J Nat Products* 75: 9–14, 2012.
30. Kietzmann T and Gorlach A. Reactive oxygen species in the control of hypoxia-inducible factor-mediated gene expression. *Semin Cell Dev Biol* 16: 474–486, 2005.
31. Korsvik C, Patil S, Seal S, and Self WT. Superoxide dismutase mimetic properties exhibited by vacancy engineered ceria nanoparticles. *Chem Commun (Camb)* 10: 1056–1058, 2007.
32. Kuchibhatla S, Karakoti AS, Bera D, and Seal S. One dimensional nanostructured materials. *Prog Mater Sci* 52: 699–913, 2007.
33. Laemmli UK. Cleavage of structural proteins during the assembly of the head of bacteriophage T4. *Nature* 227: 680–685, 1970.
34. Laurent A, Nicco C, Chereau C, Goulvestre C, Alexandre J, Alves A, Levy E, Goldwasser F, Panis Y, Soubrane O, Weill B, and Batteux F. Controlling tumor growth by modulating endogenous production of reactive oxygen species. *Cancer Res* 65: 948–956, 2005.
35. Levi F, Boffetta P, and La Vecchia C. High constant incidence rates of second primary neoplasms. *Eur J Cancer Prev* 17: 385–388, 2008.
36. Li P, Nijhawan D, Budihardjo I, Srinivasula SM, Ahmad M, Alnemri ES, and Wang X. Cytochrome c and dATP-dependent formation of Apaf-1/caspase-9 complex initiates an apoptotic protease cascade. *Cell* 91: 479–489, 1997.
37. Lin W, Huang YW, Zhou XD, and Ma Y. Toxicity of cerium oxide nanoparticles in human lung cancer cells. *Int J Toxicol* 25: 451–457, 2006.
38. Luanpitpong S, Talbott SJ, Rojanasakul Y, Nimmannit U, Pongrakhananon V, Wang L, and Chanvorachote P. Regulation of lung cancer cell migration and invasion by reactive oxygen species and caveolin-1. *J Biol Chem* 285: 38832–38840, 2010.
39. Małecki JM, Bentke A, Ostrowska B, and Laidler P. Cytochalasin D, LY294002 and olomoucine synergize in promoting death of melanoma cells through activation of caspase-3 and apoptosis. *Melanoma Res* 20: 52–58, 2010.
40. Mosmann T. Rapid colorimetric assay for cellular growth and survival: application to proliferation and cytotoxicity assays. *J Immunol Methods* 65: 55–63, 1983.
41. Nagata S. Apoptosis by death factor. *Cell* 88: 355–365, 1997.
42. Nangaku M, Izuhara Y, Takizawa S, Yamashita T, Fujii-Kuriyama Y, Ohneda O, Yamamoto M, van Ypersele de Strihou C, Hirayama N, and Miyata T. A novel class of prolyl hydroxylase inhibitors induces angiogenesis and exerts organ protection against ischemia. *Arterioscler Thromb Vasc Biol* 27: 2548–2554, 2007.
43. Parums DV, Cordell JL, Micklem K, Heryet AR, Gatter KC, and Mason DY. JC70: a new monoclonal antibody that detects vascular endothelium associated antigen on routinely processed tissue sections. *J Clin Pathol* 43: 752–757, 1990.
44. Pirmohamed T, Dowding JM, Singh S, Wasserman B, Heckert E, Karakoti AS, King JES, Seal S, and Self WT. Nanoceria exhibit redox state-dependent catalase mimetic activity. *Chem Commun* 46: 2736–2738, 2010.
45. Quiles JL, Huertas JR, Battino M, Mataix J, and Ramirez-Tortosa MC. Antioxidant nutrients and adriamycin toxicity. *Toxicology* 180: 79–95, 2002.
46. Reynolds ES. Use of lead citrate at high Ph as an electron-opaque stain in electron microscopy. *J Cell Biol* 17: 208, 1963.
47. Roberts RA, Smith RA, Safe S, Szabo C, Tjalkens RB, and Robertson FM. Toxicological and pathophysiological roles of reactive oxygen and nitrogen species. *Toxicology* 276: 85–94, 2010.
48. Ruas JL and Poellinger L. Hypoxia-dependent activation of HIF into a transcriptional regulator. *Semin Cell Dev Biol* 16: 514–522, 2005.
49. Sanchez Y, Amran D, de Blas E, and Aller P. Regulation of genistein-induced differentiation in human acute myeloid leukaemia cells (HL60, NB4) Protein kinase modulation and reactive oxygen species generation. *Biochem Pharmacol* 77: 384–396, 2009.
50. Saphir A. Angiogenesis: the unifying concept in cancer? *J Natl Cancer Inst* 89: 1658–1659, 1997.
51. Seo YH and Carroll KS. Profiling protein thiol oxidation in tumor cells using sulfenic acid-specific antibodies. *Proc Natl Acad Sci U S A* 106: 16163–16168, 2009.
52. Sies H. Strategies of antioxidant defense. *Eur J Biochem* 215: 213–219, 1993.
53. Sies H and Cadenas E. Oxidative stress—damage to intact-cells and organs. *Philos Transact R Soc London Ser B Biol Sci* 311: 617–631, 1985.
54. Stolk J, Hiltermann TJ, Dijkman JH, and Verhoeven AJ. Characteristics of the inhibition of NADPH oxidase activation in neutrophils by apocynin, a methoxy-substituted catechol. *Am J Respir Cell Mol Biol* 11: 95–102, 1994.
55. Storz P. Reactive oxygen species in tumor progression. *Front Biosci* 10: 1881–1896, 2005.
56. Stuhlmann D, Ale-Agha N, Reinehr R, Steinbrenner H, Ramos MC, Sies H, and Brenneisen P. Modulation of homologous gap junctional intercellular communication of human dermal fibroblasts via a paracrine factor(s) generated by squamous tumor cells. *Carcinogenesis* 24: 1737–1748, 2003.
57. Swietach P, Vaughan-Jones RD, and Harris AL. Regulation of tumor pH and the role of carbonic anhydrase 9. *Cancer Metastasis Rev* 26: 299–310, 2007.
58. Tang Y, Zeng X, He F, Liao Y, Qian N, and Toi M. Caveolin-1 is related to invasion, survival, and poor prognosis in hepatocellular cancer. *Med Oncol* 29: 977–984, 2012.
59. Thannickal VJ, Aldweib KDL, and Fanburg BL. Tyrosine phosphorylation regulates $H_2O_2$ production in lung fibroblasts stimulated by transforming growth factor beta 1. *J Biol Chem* 273: 23611–23615, 1998.
60. Thannickal VJ and Fanburg BL. Reactive oxygen species in cell signaling. *Am J Physiol Lung Cell Mol Physiol* 279: L1005–L1028, 2000.
61. Thompson TC, Tahir SA, Li L, Watanabe M, Naruishi K, Yang G, Kadmon D, Logothetis CJ, Troncoso P, Ren C, Goltsov A, and Park S. The role of caveolin-1 in prostate cancer: clinical implications. *Prostate Cancer Prostatic Dis* 13: 6–11, 2010.
62. Tomayko MM and Reynolds CP. Determination of subcutaneous tumor size in athymic (nude) mice. *Cancer Chemother Pharmacol* 24: 148–154, 1989.
63. Valko M, Leibfritz D, Moncol J, Cronin MT, Mazur M, and Telser J. Free radicals and antioxidants in normal physiological functions and human disease. *Int J Biochem Cell Biol* 39: 44–84, 2007.
64. Wittgen HG and van Kempen LC. Reactive oxygen species in melanoma and its therapeutic implications. *Melanoma Res* 17: 400–409, 2007.

65. Woiniak A, Drewa G, Wozniak B, Schachtschabel DO, Mila-Kierzenkowska C, Drewa T, Olszewska-Slonina D, and Soponska M. The effect of antitumor drugs on oxidative stress in B16 and S91 melanoma cells *in vitro*. *Med Sci Monit* 11: BR22– BR29, 2005.
66. Zhou M, Diwu Z, Panchuk-Voloshina N, and Haugland RP. A stable nonfluorescent derivative of resorufin for the fluorometric determination of trace hydrogen peroxide: applications in detecting the activity of phagocyte NADPH oxidase and other oxidases. *Anal Biochem* 253: 162–168, 1997.

Address correspondence to:
*Dr. Lirija Alili*
*Medical Faculty*
*Institute of Biochemistry & Molecular Biology I*
*Heinrich-Heine-University*
*40225 Duesseldorf*
*Germany*

*E-mail:* lirija.alili@web.de

Date of first submission to ARS Central, July 19, 2012; date of final revised submission, November 14, 2012; date of acceptance, December 1, 2012.

**Abbreviations Used**

αSMA = α-smooth muscle actin
A375 = human malignant melanoma cells
Cav-1 = caveoline-1
CM = conditioned medium
CNP = cerium oxide nanoparticles
$CoCl_2$ = cobalt chloride
Da = Dalton
DMEM = Dulbecco's modified Eagle's medium
DNP = dinitrophenyl
FCS = fetal calf serum
FITC = fluorescein isothiocyanate
FTIR = Fourier transform infrared spectroscopy
HBSS = Hank's balanced salt solution
HDF = human dermal fibroblast
HIF1α = hypoxia-inducible factor-1-alpha
HMEC-1 = human endothelial cells
$H_2O_2$ = hydrogen peroxide
HRP = horseradish peroxidise
HRTEM = high-resolution transmission electron microscopy
MF = myofibroblast
PARP = poly(ADP-ribose)polymerase
PBS = phosphate-buffered saline
ROS = reactive oxygen species
rTGFβ1 = recombinant transforming growth factor β1
SDS = sodium dodecyl sulfate
SDS-PAGE = sodium dodecyl sulfate–polyacrylamide gel electrophoresis
SEM = standard error of the mean
SOD = superoxide dismutase
TEM = transmission electron microscopy
XPS = X-ray photoelectron spectroscope